ISSN (Print) 1226-1750
ISSN (Online) 2233-6656
Journal of Magnetics 23(2), 238-246 (2018) https://doi.org/10.4283/JMAG.2018.23.2.238

Electromagnetic Field Characteristic Analysis and Comparison of Slotless Permanent Magnet Synchronous Generators with Grid Connection

Yu-Seop Park*

Department of Electrical Engineering, Korea National University of Transportation, Chungju 27469, Republic of Korea

(Received 10 January 2018, Received in final form 18 April 2018, Accepted 19 April 2018)

This paper deals with the characteristic analysis of permanent magnet (PM) wind power generators according to stator winding topology to compare the machine performance, and the experimentally measured current with grid connection is employed for the investigation. The analysis models dealt with in this study have the slotless structure in their stator core to eliminate the cogging torque with the identical PM rotor, and three coil winding types according to coil pitch and winding types are addressed for their comparison. One of the analysis models is manufactured to be integrated with a grid-connected power converter, and the measured phase current of the generator is applied to investigate their flux density, resulting radial force and power loss characteristics of each analysis model. For the reasonable comparison, the generators have very similar equivalent circuit parameters, such as induced voltage and resistance, so the load voltage and current characteristics are almost identical. From the results dealt with in this study, one of the analysis models is proposed to be applied for the small-scale wind power generation systems.

Keywords : Radial Flux, PM Machine, Wind Power Generator

1. Introduction

Recently, due to their high energy density and powerful performance, permanent magnet (PM) is widely applied in various electrical machines [1-3]. In particular, PM synchronous generator (PMSG) is actively applied for wind power generation systems [4-6], and, especially for its small-scale power application, the directly connected type to wind turbine is very popular due to its simple mechanical structure by eliminating gearbox. Differently from the induction generator, since PMSG does not have copper loss in its rotor, superior performance can be anticipated with relatively higher efficiency. On the other hand, compared to its axial length, this type of the generator generally has large diameter with high number of poles to be operated in relatively low speed with high torque. When it comes to the pole and slot combination of this type of machine, the authors in [7] compared various machines which were applied to direct-drive automotive starter and alternator machines. Besides, the study in [8] performed the analysis of 40 pole-48 slot permanent magnet synchronous motor with consequent pole rotor by showing the beneficial possibilities of the machine. As it is very well known, the topology of the stator coil winding can be various, and this paper deals with three winding types with the identical 40 pole PM rotor. In other words, they are respectively 1 distribution winding type and 2 concentration winding types with different coil pitch.

On the other hand, when the power converters are combined with the PM generators, the phase harmonic can have harmonic components [9]. It can be also removed by high technology of the controller, but it is still not costly effective in that many commercial power converters do not employ the system, in particular for small scale applications. Therefore, in this study, the influence of power converter with grid connection on the slotless PM wind power generators is investigated. For the comparative analysis, three models are selected according to coil pitch, and, most importantly, their equivalent circuit parameters, such as induced voltage, resistance and inductance, are almost identical so that the output power curve shows very similar values. Finally, the experimentally measured current when the manufactured model is connected to grid can be applied to other machines for comparative investigation. In this study, based on the current, related electromagnetic characteristics are performed to determine

*Corresponding author: Tel: +82-43-841-5148
Fax: +82-43-841-5140, e-mail: yspark@ut.ac.kr

the best model to be applied for the small-scale wind power generation systems.

In this paper, the analysis models according to stator coil winding types are firstly introduced in Chapter 2 while the analytical approach is employed to analyze flux density and induced voltage. In Chapter 3, one of the analysis models is manufactured for experimental verification, and it is also integrated with gird-connected power converter to measure the phase current of the generator. Since the phase current of the generator when it is connected to grid, the harmonics have high influence on generator performance. Therefore, its relevant investigation including power loss characteristics and radial force is addressed as well. Lastly, in Chapter 4, the conclusion is made based on the analysis results and discussions presented in this study.

2. Electromagnetic Field Analysis of PMSGs According to Stator Coil Pitch

2.1. Analysis Models

In Fig. 1, the analysis models addressed in this paper are presented, and they have identical rotor structure with different winding topology. In other words, the number of poles is 40 for each model while three phase coil winding is attached in the stator core with Y-connection. The stator core is slotless type to eliminate the cogging torque which is very important for the initial operations in low wind speed condition. Here, the coil pitch (CP) of Type A, Type B and Type C is respectively 9.0(deg.), 7.5(deg.) and 6.0(deg.) according to winding types as shown in the figures. The main objective to determine the analysis models is to investigate the influence of the grid-connected power converter on the distributed winding and concentration winding machines as well as the integer and fractional combination. Although the analysis models are slotless machine, if it is assumed that the slots are existed, the pole and slot combination of Type A is 40 poles and 120 slots while that of Type C is 40 poles and 60 slots. They are typical distribution winding and concentration winding with integer combination. However, the Type B has 40 pole and 48 slots which fractional pole and slot combination. Therefore, the analysis models consider the distribution winding and the concentration winding as well as the integer combination and the fractional combination. Most importantly, under the size limitation of the outer diameter and inner diameter, those models are designed to have almost identical equivalent circuit parameters, such as induced voltage in no-load condition and resistance, so that their output power curve has no difference for the reasonable comparison. Furthermore, under the size limitation, the number of coils and stack length are designed to meet the requirements, and more detailed specifications are provided in Table 1. As can be confirmed, the resistance are very similar, and the minor difference of the induce values does not have high influence on the comparison in that the machines are operated in very lower speed condition as will be presented later. Furthermore, the maximum output power is 0.4(kW), and the wind turbine can be operated to 150(rpm). The power curve of the grid-connected power converter is presented in Fig. 2, and the speed range under 80(rpm) is operated

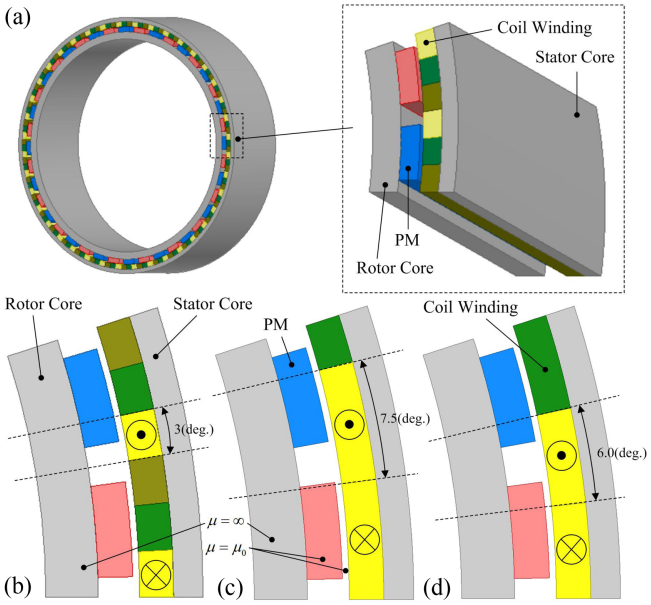

Fig. 1. (Color online) Analysis models with identical rotor structure according to winding topology: (a) entire view, (b) Type A (CP = 9.0(deg.)), (c) Type B (CP = 7.5(deg.)), (d) Type C (CP = 6.0(deg.)).

Table 1. Design Specification of Analysis Models.

Specification	Unit	Type A	Type B	Type C
Maximum Output Power	kW	0.4	0.4	0.4
Maximum Speed	rpm	150	150	150
Number of Poles	-	40	40	40
Coil Pitch of Winding	deg.	9	7.5	6
Outer Diameter of Stator	mm	286	286	286
Inner Diameter of Stator	mm	277	277	277
Outer Diameter of Rotor	mm	254	254	254
Inner Diameter of Rotor	mm	238	238	238
Stack Length	mm	85	166	133
Turns per Phase	turns	760	520	650
Resistance	ohm	12.09	12.07	12.09
Inductance	mH	4.1	7.7	6.5
Power Density	W/mm^2	13651.52	26594.12	21254.34

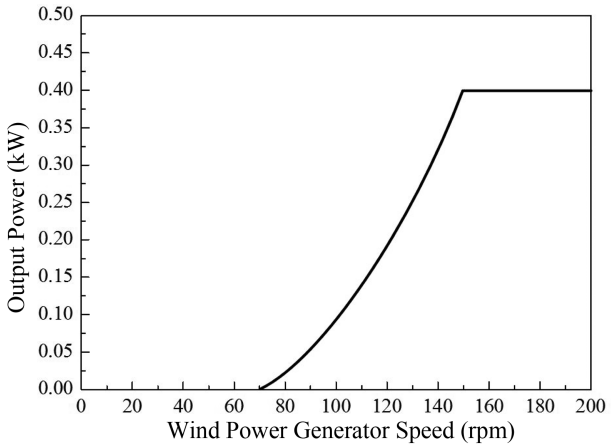

Fig. 2. Output power curve of gird-connected power converter according to rotational speed of wind power PMSG.

as no-load condition without any current in the generator. As can be confirmed in the figure, the output power is increased according to the rotational speed increment by controlling the output current while the output voltage is constant to be 220(V) and 60(Hz). More specific explanation will be presented later with experimentally measured waveforms.

2.2. Electromagnetic Field Analysis for Derivation of Flux Density and Induced Voltage

For the characteristic analysis of open circuit field based on analytical method, the analysis models presented in Fig. 1 can be considered by the simplified layers with their permeability as indicated in the figure, and Maxwell's equations are employed to derive governing equation [10]. At first, by using the relationship between magnetic flux density $\boldsymbol{B}$, magnetic field intensity $\boldsymbol{H}$ and magnetization $\boldsymbol{M}$, (1) can be derived, and it can be also rewritten as (2) by using the definition of magnetic vector potential. Here, the magnetic vector potential $\boldsymbol{A}$ is expressed by (3) while k is obtained by multiplying harmonic coefficient n and the number of pole pairs p. Furthermore, the magnetization $\boldsymbol{M}$ can be expressed by (4) with pole arc ratio α_r. Here, $\boldsymbol{M_r}$ and $\boldsymbol{M_\theta}$ are respectively the radial component and tangential component of the magnetization.

$$\nabla \times \mathrm{B} = \mu_0(\nabla \times \mathrm{M}), \quad \mathrm{B} = \nabla \times \mathrm{A} \tag{1}$$

$$\frac{\partial^2}{\partial r^2}A + \frac{1}{r}\frac{\partial}{\partial r}A + \frac{1}{r^2}\frac{\partial^2}{\partial \theta^2}A + \frac{\partial^2}{\partial z^2}A = -\mu_0(\nabla \times \mathrm{M}) \tag{2}$$

$$\mathrm{A} = A_{zn}(r)e^{j(k\theta)}\mathrm{i}_z \quad (k = np) \tag{3}$$

$$\mathrm{M} = \sum_{n=-\infty,odd}^{\infty} \alpha_r \left[M_{rn}e^{jnp\theta}\mathrm{i}_r + M_{\theta n}e^{jnp\theta}\mathrm{i}_\theta \right] \tag{4}$$

On the other hand, since the right side of (1) can be derived as (5), the homogeneous solution and the particular solution are derived as (6) and (7), respectively. In (6), A_1 and A_2 are derived by calculating the homogeneous solution in the layer of the PM.

$$\nabla \times \mathrm{M} = \frac{\mu_0}{r}(M_{\theta n} - jkM_{rn})e^{jk\theta} \tag{5}$$

$$A_{znh} = \sum_{n=-\infty,odd}^{\infty} \left[A_1 r^k + A_2 r^{-k} \right] \tag{6}$$

$$A_{znp} = \sum_{n=-\infty,odd}^{\infty} \frac{jr\mu_0 k(M_{rn} + M_{\theta n}/jk)}{1-(k)^2} e^{jk\theta} \tag{7}$$

As a result, the radial component and tangential component of flux density can be obtained as (8) and (9) by calculating right side of (1). Based on those equations, the magnetic vector potential of each region can be obtained by applying boundary conditions. In addition, the induced voltage considering the coil pitch of stator winding can be achieved by deriving the magnetic vector potential in coil layer as presented in (10). Here, N is the number of turns, and L is the stack length.

$$B_{rn} = \frac{jk}{r}A_{zn}e^{jk\theta} \tag{8}$$

$$B_{\theta n} = -\frac{\partial}{\partial r}A_{zn}e^{jk\theta} \tag{9}$$

$$e = -jk\omega NLA_{zn\_coil}\left[e^{jk(\theta+\omega t)} - e^{jk\omega t} \right] \tag{10}$$

Figure 3 presents the analyzed radial component and tangential component of flux density, and the induced voltage waveform at 150(rpm) is presented in Fig. 4. As can be confirmed in the figure, the analysis models have almost identical values while their FFT results in Fig. 5 supports the design results. In the figure, Type A has a bit more harmonics than the others, but it is very minor

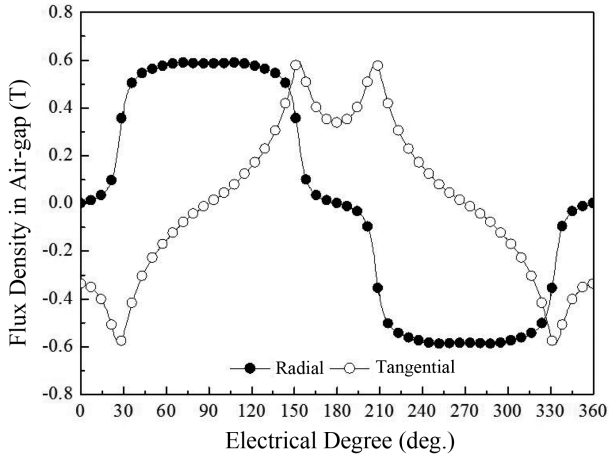

Fig. 3. Radial component and tangential component of flux density in air-gap.

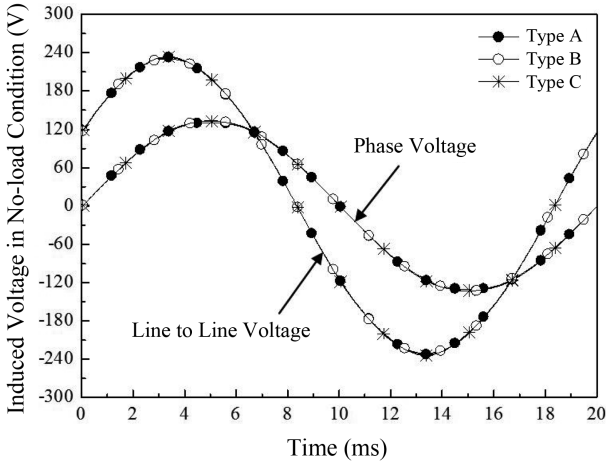

Fig. 4. Induced voltage in no-load condition of analysis models according to winding topology at 150(rpm).

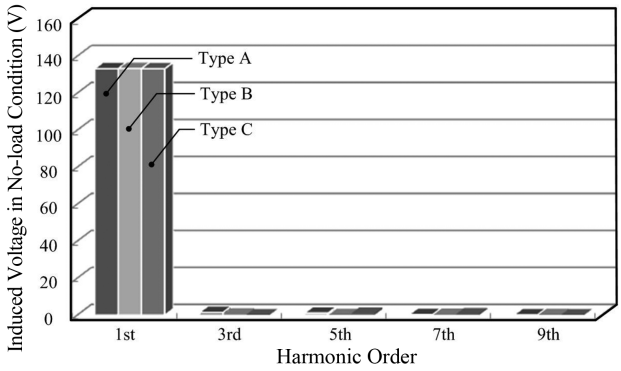

Fig. 5. FFT results of phase induced voltage according to motor types in no-load condition at 150(rpm).

difference which can be neglected.

2.3. Power Curve Comparison according to Generator Types

In this study, based on the derived generator parameters, such as induced voltage in no-load, resistance and inductance, the power curve of PMSG is determined by the equivalent circuit method by deriving load voltage and phase current [10]. In other words, the equivalent circuit and vector diagram is presented in Fig. 6, and the output power curve can be obtained by (11)-(13) based on the figures and equations. Here, V_L, E_0, R_{ph}, R_{load}, X_s, I_{ph} and P_{out} are respectively load voltage, induced voltage, phase resistance, load resistance, synchronous reactance, phase current and output power.

$$V_L = \frac{E_0\left(\sqrt{(R_{ph}+R_{load})^2+X_s^2}-\sqrt{R_{ph}{}^2+X_s^2}\right)}{\sqrt{(R_{ph}+R_{load})^2+X_s^2}} \tag{11}$$

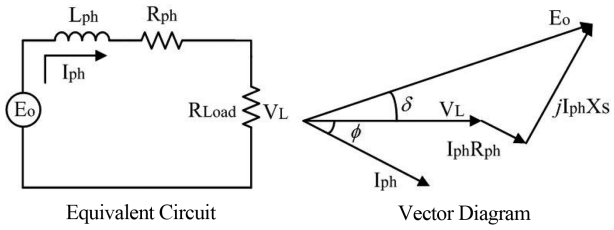

Fig. 6. Equivalent Circuit and vector diagram of PMSG to derive output power curve based on derived parameters.

$$I_{ph} = \frac{E_0}{\sqrt{(R_{ph}+R_{load})^2+X_s^2}} \tag{12}$$

$$P_{out} = 3 \cdot V_{L\cdot rms} \cdot I_{ph\cdot rms} \tag{13}$$

On the other hand, based on the derived equivalent circuit parameters, the output voltage versus current according to rotational speed are presented in Fig. 7. As can be anticipated, the analysis models show almost identical characteristics. In addition, as will be presented later, the measured value of Type A also supports the validity of the analysis results.

3. Comparative Investigation on Influence of Grid-Connected Power Converter with Experimentally Measured Generator Current

3.1. Manufactured Machine

As shown in Fig. 4, Fig. 5, Fig. 7 and Table 1, the machines have almost identical machine performance in no-load and AC load condition. In other words, it indicates that the machines have identical current values regardless

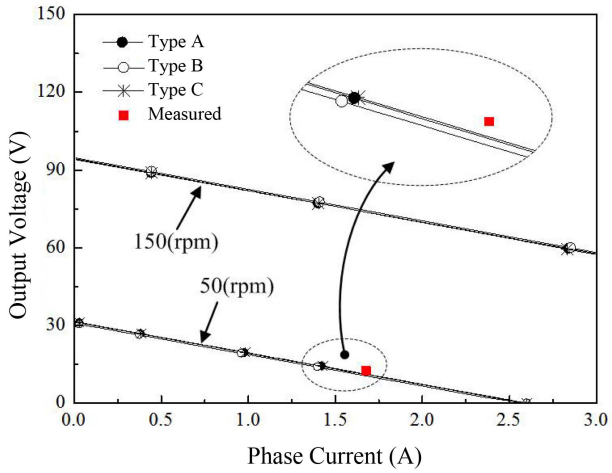

Fig. 7. (Color online) Output voltage and current characteristics versus rotational speed of machines based on vector diagram and equivalent circuit.

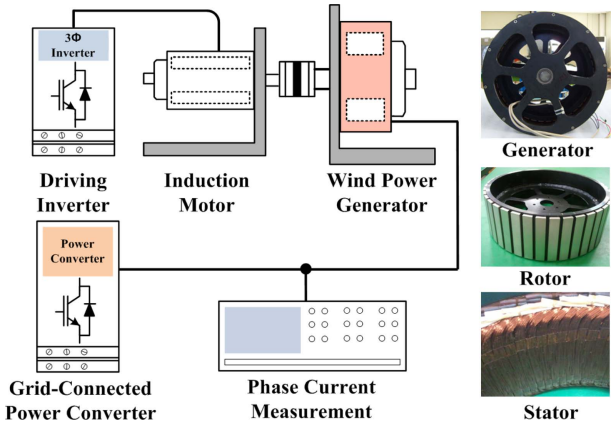

Fig. 8. (Color online) Experimental set construction with manufactured machine (Type A).

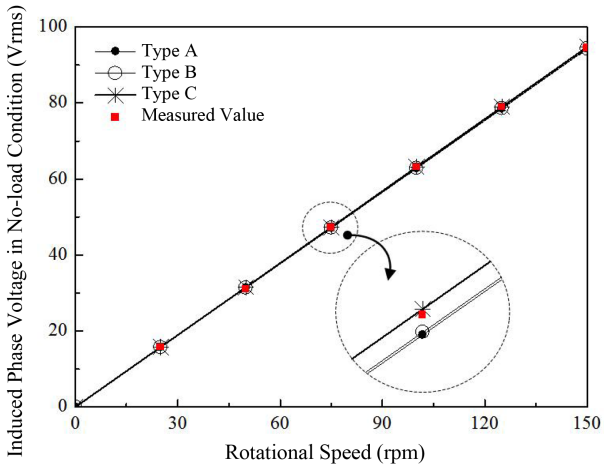

Fig. 9. (Color online) Comparison of induced phase according to rotational speed and experimental verification with manufactured PMSG.

of the variation of the load conditions. On the other hand, in a view point of the machine volume, since the Type A has the shortest stack length, its energy density is highest as shown in the Table 1. The volume has also close relevance to cost and weight. Therefore, it was determined that Type A with distribution winding is selected to be manufactured. The validity of the analysis results can be demonstrated by the measured values presented in Fig. 7. Besides, with the manufactured machine, experimental set was constructed with grid connection, and the voltage of the grid is 220(V) and 60(Hz).

As presented in Fig. 8, the wind power generator is directly connected to an induction motor for the artificial mechanical input power while the speed of the generator is controlled by the driving inverter. On the other hand, the wind power generator is integrated with the grid-connected power converter so that the generator current is measured while the generated electrical energy is connected to grid. First of all, for the verification of the analysis results, the induced voltage of the manufactured machine is measured according to the rotational speed as shown in Fig. 9. In the experiment, the power converter is not connected to the three phase winding of the generator and the phase current could be measured by using neutral line which additionally made for the measurement. On the other hand, from the figure, it can be confirmed that the values are very well corresponded. Beside, for the load condition, the relevant experiment is also performed, and the measured output voltage and phase current are indicated in Fig. 7. The experiment was performed at 50(rpm) of rotational speed condition, and the load resistance was 7.5(ohm) for each phase. As a result, from the experiment in no-load and load conditions, since the analysis results and the measured values are very similar, the validity of the electromagnetic field analysis can be demonstrated.

3.2. Integration of Manufactured Wind Power Generator with Grid-Connected Power Converter

As mentioned above, the analysis model is for the integration with grid-connected power converter, which is the single phase of 220(V) and 60(Hz). From the electromagnetic field analysis results, it was confirmed that the analysis models have almost identical equivalent circuit parameters regardless of the machine size and stator winding types by showing very little difference of the voltage and current values. Therefore, it can be also anticipated that the generator current must be almost identical when the grid-connected power converter is integrated with the machines, so the experimentally measured current of Type A can be also applied to other machines for their

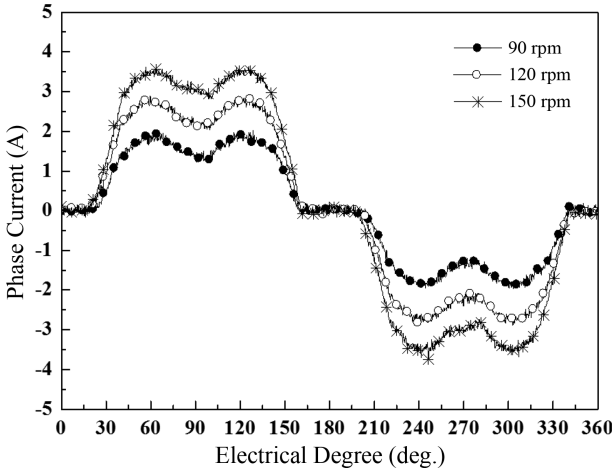

Fig. 10. Measured phase current of PMSG according to speed conditions.

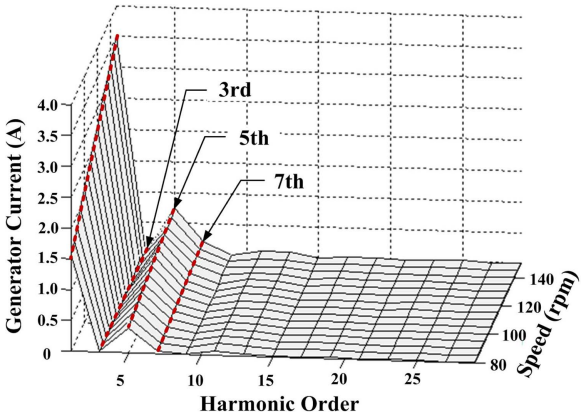

Fig. 11. (Color online) FFT results of measured current according to speed conditions.

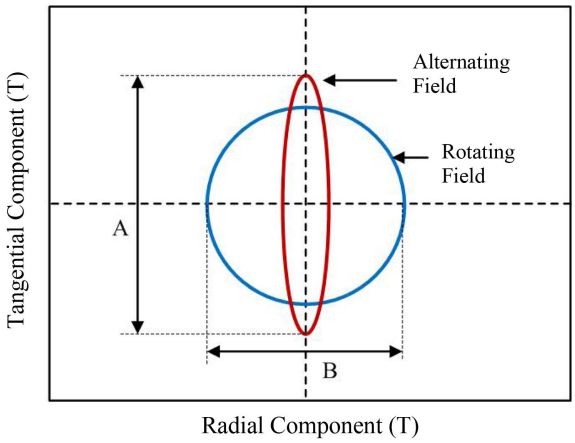

Fig. 12. (Color online) Analyzed points to achieve radial and tangential component of flux density in stator core.

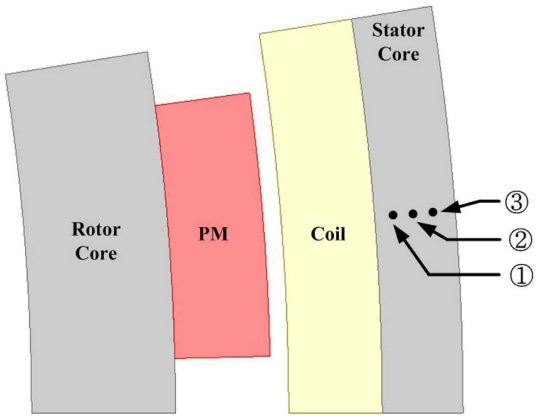

Fig. 13. (Color online) Analyzed points to achieve radial and tangential component of flux density in stator core.

comparative investigation. With the constructed experimental set mentioned above, the phase current of the generator is measured. For instance, Fig. 10 compares measured current characteristics when the rotational speed of the generator is varied from 90(rpm) to 120(rpm). Here, the output gird voltage is controlled to be 220(V) while the current is controlled according to the rotational speed of the generator. Most importantly, due to the diode rectifier, the generator line-to-line voltage does not have sinusoidal waveform, and the current contains harmonics. According to the generator speed conditions, since the output power is increased with the rotational speed of the generator, higher current is measured when the speed is increased. Furthermore, the Fast Fourier Transform (FFT) results are presented in Fig. 11, and it can be confirmed that the 5th harmonic component is being increased as the rotational speed of the generator increases. The figure also presents the other harmonic components, such as the 3rd and 7th components, varies less than the 5th component.

3.3. Magnetic Behavior and Radial Force Characteristics

Based on the measure current, electromagnetic field analysis is performed, and the magnetic behavior is comparatively investigated in the various position of the slotless stator core. At first, the magnetic behavior can be largely divided into the alternating field and rotating field as shown in Fig. 12. In other words, the magnetic behavior is defined as the ratio A to B while the rotating filed is determined when the ratio is over 2 in this study. As presented later, the core loss due to the rotating field is twice than the alternating field in the modified Steinmetz equation. Figure 13 presents the analysis points to achieve magnetic flux density. As presented in the previous study [9], the harmonic components of the flux density have high influence on the core loss characteristics. Since the analysis models have identical rotor and stator except for the coil winding, the figure can be applied to all the models. Consequently, as shown in Fig. 14, the analysis results of radial component and the tangential component at point 1, 2, and 3 are compared according to machines types. Since the phase current does not exist, the flux density is not distorted in the no-load condition. However, with the phase current influenced by the grid connected power converter, the flux density contains harmonics. As presented in [11], the flux density distribution has also very close correlation with the radial force which is the electromagnetic source of the vibration and noise. The radial force can be calculated by the derived radial component and tangential component of flux density. Figure 15 presents the analyzed radial force according to machine types, and it can be confirmed that Type B

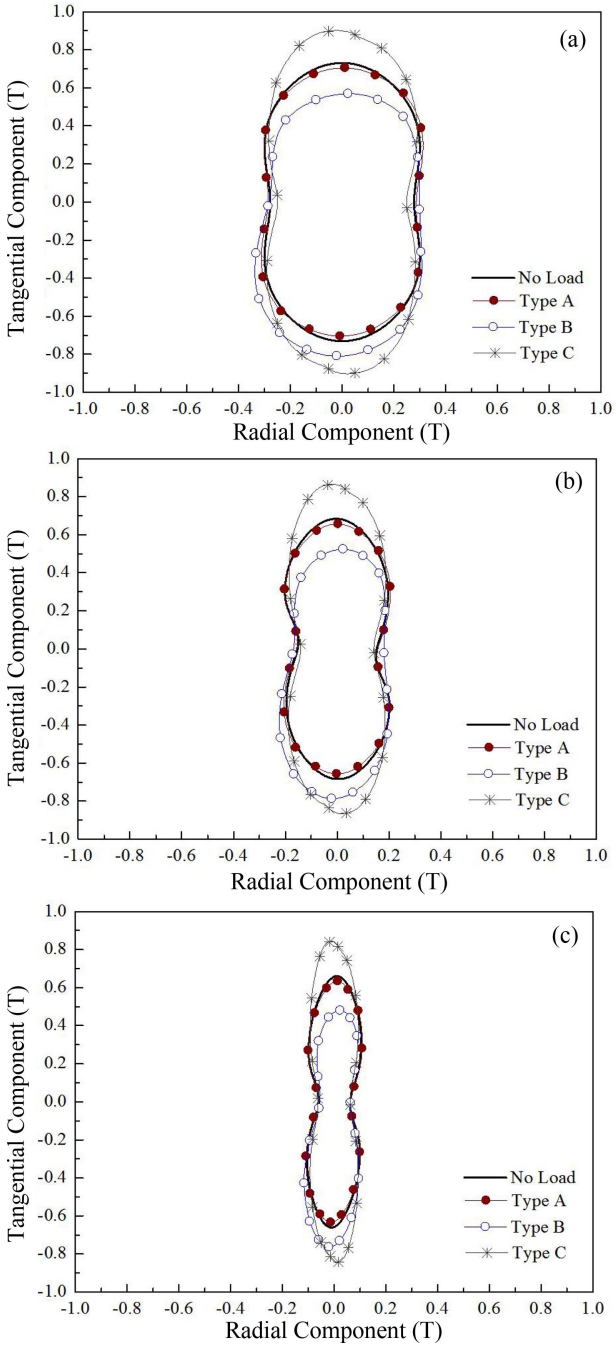

Fig. 14. (Color online) Radial component and tangential component of flux density influenced by measured current: (a) point 1, (b) point 2, (c) point 3.

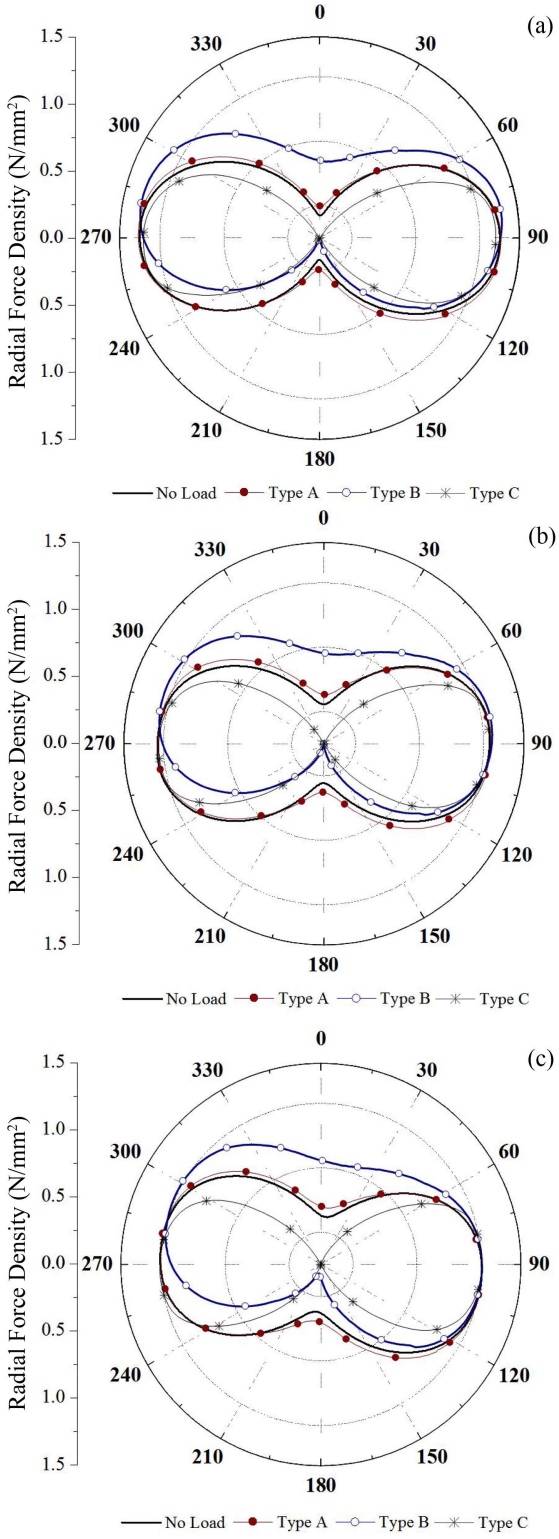

Fig. 15. (Color online) Radial force distribution influenced by grid-connected power converter according to machine types: (a) Point 1, (b) Point 2, (c) Point 3.

shows the relative larger distortion in that the others have regular distribution.

3.4. Power Loss Comparison according to Generator Types

Based on the measured current, the power losses of each generator are analyzed. As presented in previous study [10], the copper loss can be calculated by (14) while the core loss is estimated by the modified Steinmetz

equation (15). Here, l is the harmonic order and Q indicates the magnetic behavior. In other words, $Q = 1$ is the alternating filed and $Q = 2$ is the rotating field. Besides, k_h, k_e and k_{ex} are the hysteresis, eddy current and excess loss constant, respectively. The rotor loss is derived by applying the measured current based on FEM.

$$P_{copper} = 3R_{ph}\sum_{l=1}^{\infty} I_l^2 \tag{14}$$

$$P_{core} = \sum_{l=1}^{\infty} Q_l (k_{hl} f_l B_l^n + k_{el} f_l^2 B_l^2 + k_{al} f_l^{1.5} B_l^{1.5}) \tag{15}$$

In Fig. 13, it can be known that the magnetic behavior is different according to the position of the stator core despite the slotless machine. In other words, the rotating field is dominant in point 1 while the alternating field is much more dominant in point 3 of the stator core. As presented above, the core loss with rotating field generates twice, and this is visible when the position access to the mechanical air-gap.

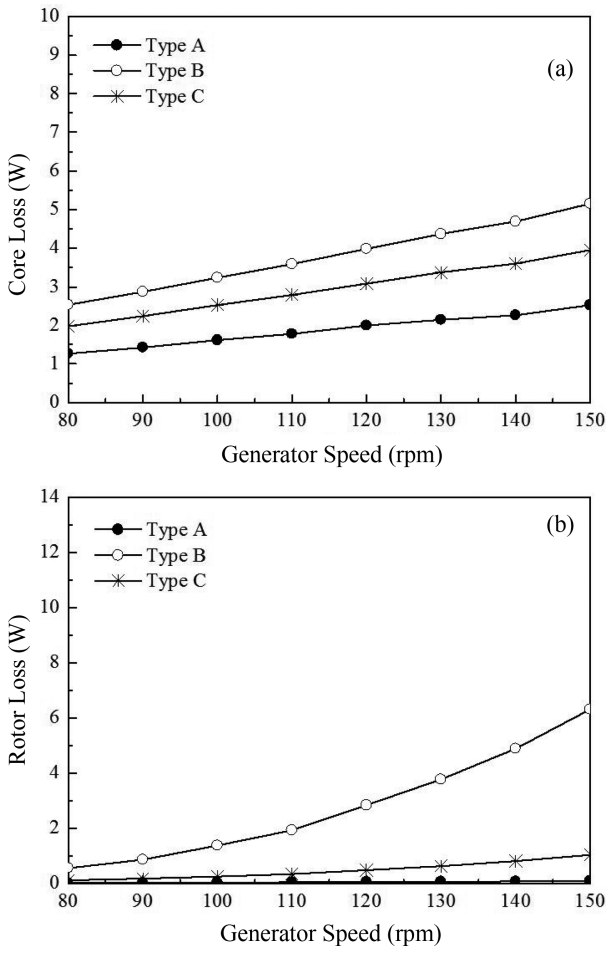

Fig. 16. Power loss comparison according to rotational speed conditions: (a) core loss, (b) rotor loss.

Lastly, in Fig. 16, the analyzed power losses are compared according to the machine types and rotational speed condition when the machines are operated with the grid-connected power converter. As mentioned above, it was confirmed that the generators have identical current characteristics in spite of the winding topology, the measured current of the manufactured machine Type A was identically employed in the other machines for the calculation. At first, when it comes to core loss characteristics, Type B shows highest value as the speed reaches to 150(rpm) while the difference is much lower when the generators are operated in low speed conditions. On the other hand, as can be confirmed in the figure, Type B also shows very high value of rotor loss in comparison with the others. From the results, it can be confirmed that Type B is not appropriate for the grid-connected wind power generation system.

4. Conclusion

In this paper, the comparative investigation of PMSGs for small-scale wind power generator applications is performed considering stator coil winding based on electromagnetic field analysis. For the reasonable comparison, each machine has almost identical equivalent circuit parameters, so the measured current of the manufactured machine was employed to investigate the influence of the gird-connected power converter. From the analysis results of flux density, radial force and power loss, the Type B, which coil pitch is 7.5(deg.) is not appropriate decision in that its relatively larger distorted radial force distribution, core loss and rotor loss characteristics. In particular, when it comes to core loss, Type A showed lower values of 48.9(%) and Type C showed lower values of 76.7(%) compared to Type B in the 150(rpm) of rotational speed condition. For the core loss, the difference of low speed and high speed conditions is not high. On the other hand, the rotor loss presented different trend according the speed variation. Type A showed very similar rotor loss variation according to rotational speed conditions while its values are lowest, but Type B showed very visible difference in 150(rpm) of rotational speed condition.

Acknowledgment

This was supported by Korea National University of Transportation in 2018, and this work was supported by the National Research Foundation of Korea (NRF) grant funded by the Korea government (MSIP; Ministry of Science, ICT & Future Planning) (No. 2017R1C1B5015907).

References

[1] S. I. Kim, J. P Hong, J. Magn. **21**, 405 (2016).
[2] J. H. Yoo and T. U. Jung, J. Magn. **21**, 249 (2016).
[3] J. Ikram, N. Khan, Q. Junaid, S. Khaliq, and B. I. Kwon, J. Magn. **22**, 257 (2017).
[4] J. Chen, C. V. Nayar, and L. Xu, IEEE Trans. Magn. **36**, 5 (2000).
[5] Y. Chen, P. Pillay, and A. Khan, IEEE Trans. Ind. Appl. **41**, 6 (2005).
[6] L. Jian, K. T. Chau, and J. Z. Jiang, IEEE Trans. Ind. Appl. **45**, 3 (2009).
[7] A. M. EL-Refaie and T. M. Jahns, IEEE Trans. Energy Convers. **21**, 2 (2006).
[8] S. U. Chung, J. M. Kim, D. H. Koo, B. C. Woo, D. K. Hong, and J. Y. Lee, IEEE Trans. Magn. **48**, 11 (2012).
[9] H. Polinder and M. J. Hoeijmakers, IEEE Proc.-Electr. Power Appl. **146**, 3 (1999).
[10] Y. S. Park, M. M. Koo, S. M. Jang, H. I. Park, and J. Y. Choi, IEEE Trans. Energy Convers. **28**, 4 (2013).
[11] T. Sun, J. M. Kim, G. H. Lee, J. P. Hong, and M. R. Choi, IEEE Trans. Magn. **47**, 5 (2011).